MODELING 3D WAVE PROPAGATION IN THE OCEAN COUPLED WITH ELASTIC BOTTOM AND IRREGULAR INTERFACE

LI-WEN HSIEH[1], DING LEE[2], AND CHI-FANG CHEN[1]

[1] *Department of Engineering Science and Ocean Engineering, National Taiwan University*
http://uwaclab.na.ntu.edu.tw

[2] *Naval Undersea Warfare Center*
DingLee1@aol.com

In the past few decades the elastic properties of ocean bottom were usually ignored to simplify problems by assuming a fluid seabed. Nevertheless, while it is acceptable to make such assumptions in deep water, the effects of shear waves can never be omitted as long as sound waves penetrates into ocean bottom, especially in shallow water where interactions between sound waves and elastic bottom are very frequent. Hence, seabed has to be considered as elastic solids to correctly reveal the propagating behavior of sound waves. A novel mathematical model and an implicit finite difference method to obtain a numerical solution for predicting wave propagation in a 3D ocean coupled with irregular fluid/solid interface are presented and developed into a computer code. Theoretical and computational aspects of the proposed parabolic equation solution procedure are investigated. Several numerical examples are included to show satisfactory results after comparing to known reference solutions with shear effects.

1 Introduction

In 1989, Shang and Lee [2] introduced a model to treat the two-dimensional fluid/solid horizontal interface following Ref. [11]. This model is limited to solving narrow-angle, two-dimensional horizontal interface problems. Moreover, no solution of elastic PE was incorporated into the fluid model. Later In 1998, Lee *et al.* [3] extended the Shang-Lee model to handle the horizontal fluid/solid interface three-dimensionally. Their approach is to transform the fluid/solid interface for the Helmholtz equation into the conditions suitable for the PE. A mathematical model was formulated to predict wave propagation in a coupled three-dimensional fluid/solid media. In 1999, a numerical solution to this horizontal fluid/solid interface model was introduced by Sheu *et al.* [4] who used a finite difference technique to solve the above wave equation using a predictor-corrector procedure. In 2002, Nagem and Lee [6] extended the horizontal fluid/solid interface model to handle the irregular fluid/solid interface. However, after closely following their procedure, serious mistakes are found so that their results can not be adopted. Therefore this dissertation is based on the same fundamental relations and theories with Nagem's work but subsequent derivation is novel.

An efficient numerical model for 3D wave propagation in the ocean coupled with elastic bottom and irregular interface by a PE method and a stable ODE solver is to be developed. First the mathematical model is formulated, and then a computational model which can generate a satisfactory solution using an accurate and stable numerical method is developed in this dissertation. This model is designed and capable not only for coupled 3D ocean acoustic wave propagation, but also for propagation in pure fluid or elastic solids, provided the initial and boundary conditions as well as other environmental variables are properly defined. Results of some examples with analytic solutions are also reported in this dissertation to validate the model and to show the shear wave effects. A 3D test case is also given to exhibit 3D effects.

The paper is organized as follow. Section 2 derives the representative fluid/solid coupled wave equations written in operator form. Following the theoretical formulation summary, Sec. 3 briefly presents the development of the computational model. The theoretical and computational aspects of the numerical algorithm and the resultant difference equations are given. Section 4 is devoted to validate the numerical model by several test cases. Summary of this paper is given in Sec. 5 remarking the major conclusions and directions for future works. This paper is partly extracted from the first author's Ph.D. dissertation [16].

2 Theoretical Derivation

In this section, the theoretical part for the proposed numerical model is briefly reviewed. A mathematical model has been developed by Lee *et al.* [3] which introduced a set of 3D fluid/solid coupled wave equations. However, an alternative mathematical model is derived in this paper instead of direct applying their result. A summary of this set of equations is given in operators form of a set of parabolic equations. This summary outlines the mathematical model involving the fluid wave equation, a set of interface vector equations, and the elastic wave equations.

To be adapted for parabolic equation approximation, the displacement potentials written in cylindrical coordinates can be related to the elastic potential functions by [12]

$$\phi = r^{-\frac{1}{2}} A e^{ik_L r}, \quad \psi_r = r^{-\frac{3}{2}} B_r e^{ik_T r}, \quad \psi_\theta = r^{-\frac{1}{2}} B_\theta e^{ik_T r}, \quad \psi_z = r^{-\frac{1}{2}} B_z e^{ik_T r}. \quad (2.1)$$

2.1 Parabolic Elastic and Fluid Wave Equations in Operator Form

If the potential functions expressions (2.1) are substituted into the wave equations, and considering the zero-divergence condition along with far-field approximation, rearrangement of the results gives

$$\begin{aligned}
&\frac{\partial^2 A}{\partial r^2} + 2ik_L \frac{\partial A}{\partial r} + \frac{\partial^2 A}{\partial z^2} + \frac{1}{r^2}\frac{\partial^2 A}{\partial \theta^2} = 0, \quad \frac{\partial^2 B_z}{\partial r^2} + 2ik_T \frac{\partial B_z}{\partial r} + \frac{\partial^2 B_z}{\partial z^2} + \frac{1}{r^2}\frac{\partial^2 B_z}{\partial \theta^2} = 0, \\
&\frac{\partial^2 B_r}{\partial r^2} + 2ik_T \frac{\partial B_r}{\partial r} + \frac{\partial^2 B_r}{\partial z^2} + \frac{1}{r^2}\frac{\partial^2 B_r}{\partial \theta^2} = -2\frac{\partial B_z}{\partial z}, \\
&\frac{\partial^2 B_\theta}{\partial r^2} + 2ik_T \frac{\partial B_\theta}{\partial r} + \frac{\partial^2 B_\theta}{\partial z^2} + \frac{1}{r^2}\frac{\partial^2 B_\theta}{\partial \theta^2} = -\frac{2}{r^3}\frac{\partial B_r}{\partial \theta}.
\end{aligned} \quad (2.2)$$

Equations in (2.2) are second-order partial differential in the variable r, but each can be separated into two uncoupled first order parabolic equations [12], one equation representing waves which propagate in the direction of increasing r, and the other equation representing waves which propagate in the direction of decreasing r. The separation gives the elastic outgoing wave equations in operator form

$$\begin{aligned}
&\left(\frac{\partial}{\partial r} + ik_L - ik_L\sqrt{1+L_L}\right)A = 0, \quad \left(\frac{\partial}{\partial r} + ik_T - ik_T\sqrt{1+L_T}\right)B_r = \frac{1}{2ik_T\sqrt{1+L_T}}\left(-2\frac{\partial B_z}{\partial z}\right), \\
&\left(\frac{\partial}{\partial r} + ik_T - ik_T\sqrt{1+L_T}\right)B_z = 0, \quad \left(\frac{\partial}{\partial r} + ik_T - ik_T\sqrt{1+L_T}\right)B_\theta = \frac{1}{2ik_T\sqrt{1+L_T}}\left(-\frac{2}{r^3}\frac{\partial B_r}{\partial \theta}\right),
\end{aligned} \quad (2.3)$$

where the operators are defined as

$$L_L \equiv \frac{1}{k_L^2}\left(\frac{\partial^2}{\partial z^2}+\frac{1}{r^2}\frac{\partial^2}{\partial \theta^2}\right), \quad L_T \equiv \frac{1}{k_T^2}\left(\frac{\partial^2}{\partial z^2}+\frac{1}{r^2}\frac{\partial^2}{\partial \theta^2}\right). \tag{2.4}$$

Rearrangement of Eq. (2.3) gives the parabolic elastic wave equations in a matrix form

$$\frac{\partial}{\partial r}\begin{pmatrix} A \\ B_z \\ B_r \\ B_\theta \end{pmatrix} = \begin{bmatrix} \mathrm{A}_L & 0 & 0 & 0 \\ 0 & \mathrm{A}_T & 0 & 0 \\ 0 & \mathrm{B}_T\left(-\frac{\partial}{\partial z}\right) & \mathrm{A}_T & 0 \\ 0 & 0 & \mathrm{B}_T\left(-\frac{1}{r^3}\frac{\partial}{\partial \theta}\right) & \mathrm{A}_T \end{bmatrix} \begin{pmatrix} A \\ B_z \\ B_r \\ B_\theta \end{pmatrix}, \tag{2.5}$$

where the operators in coefficients are defined as

$$\mathrm{A}_L = ik_L\left(-1+\sqrt{1+L_L}\right), \quad \mathrm{A}_T = ik_T\left(-1+\sqrt{1+L_T}\right), \quad \mathrm{B}_T = \frac{1}{ik_T\sqrt{1+L_T}}. \tag{2.6}$$

A fluid can be regarded as an elastic material of no rigidity, therefore the fundamentals and derivations of the wave equations for both media are the same. Thus for fluid, Eq. (2.5) reduces to

$$\frac{\partial}{\partial r}\left(A_f\right) = \left[\mathrm{A}_f\right]\left(A_f\right), \tag{2.7}$$

where the operator is defined as

$$\mathrm{A}_f \equiv ik_f\left[-1+\sqrt{1+\frac{1}{k_f^2}\left(\frac{\partial^2}{\partial z^2}+\frac{1}{r^2}\frac{\partial^2}{\partial \theta^2}\right)}\right], \tag{2.8}$$

and k_f is the fluid wave number.

2.2 *Parabolic Interface Vector Equations in Operator Form*

For the formulation of the irregular fluids-elastic interface conditions, a set of unit vectors must be defined which describes the geometry of an arbitrary orientation. This set of vectors is defined by:

$\eta\left(\eta_r, \eta_\theta, \eta_z\right)$ is the unit vector normal to interface;

$\mathbf{t}\left(t_r, t_\theta, t_z\right)$ is the unit vector in plane of the interface;

$\mathbf{s}\left(s_r, s_\theta, s_z\right)$ is the second vector in the tangent plane of the interface perpendicular to $\mathbf{t}$.

Along with the orientation vectors, the irregular fluid/solid interface conditions are formulated by means of tensor vectors as

$$\mathbf{u}_e^T\boldsymbol{\eta} = \mathbf{u}_f^T\boldsymbol{\eta}, \quad p_f = -\boldsymbol{\eta}\boldsymbol{\sigma}^T\boldsymbol{\eta}, \quad \mathbf{t}^T\boldsymbol{\sigma}\boldsymbol{\eta} = 0, \quad \mathbf{s}^T\boldsymbol{\sigma}\boldsymbol{\eta} = 0. \tag{2.9}$$

In practice, the geometry can be simplified by introducing the cylindrical sloping interface where the angle to the slope is ϑ, and the specific orientations are defined in following, as shown in Fig. 2.1.

►For the horizontal interface, $\boldsymbol{\eta}=(0,0,1)$, $\mathbf{t}=(1,0,0)$, and $\mathbf{s}=(0,1,0)$.

►For the irregular cylindrical sloping interface, $\boldsymbol{\eta}=(-\sin\vartheta,0,\cos\vartheta)$, $\mathbf{t}=(\cos\vartheta,0,\sin\vartheta)$, and $\mathbf{s}=(0,1,0)$.

If $\vartheta=0$, the irregular interface cases are all reduced to the case of horizontal interface. Note that $\eta_r^2+\eta_z^2=\eta_z t_r-\eta_r t_z=\cos^2\vartheta+\sin^2\vartheta=1$.

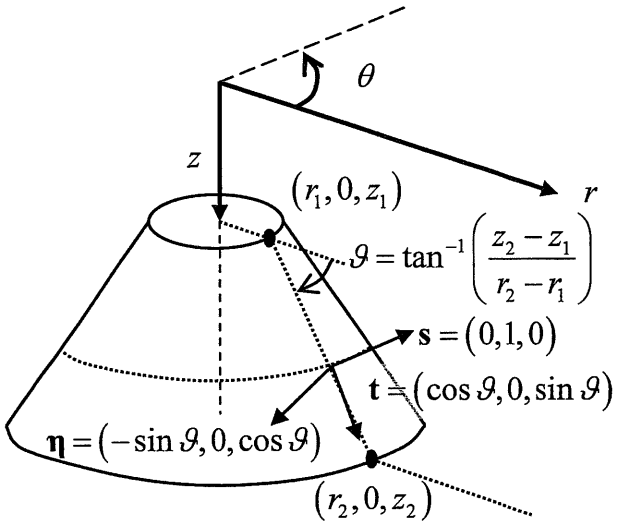

Fig. 2.1 Schematic of irregular cylindrical sloping interface

For the orientations introduced in the above, the general irregular interface conditions are simplified to give explicitly

$$-\sin\vartheta u_f+\cos\vartheta w_f=-\sin\vartheta u_e+\cos\vartheta w_e, \tag{2.10}$$

$$-p_f=\sin^2\vartheta\sigma_{rr}-2\sin\vartheta\cos\vartheta\sigma_{rz}+\cos^2\vartheta\sigma_{zz}, \tag{2.11}$$

$$\left(\cos^2\vartheta-\sin^2\vartheta\right)\sigma_{rz}=\sin\vartheta\cos\vartheta\left(\sigma_{zz}-\sigma_{rr}\right), \tag{2.12}$$

and

$$\sin\vartheta\sigma_{r\theta}=\cos\vartheta\sigma_{\theta z}. \tag{2.13}$$

Further simplification can be made by combining Eqs. (2.11) and (2.12) to eliminate σ_{rr}. The following equation is obtained where σ_{rr} is involved implicitly:

$$-\cos\vartheta p_f=-\sin\vartheta\sigma_{rz}+\cos\vartheta\sigma_{zz}. \tag{2.14}$$

Solving the interface conditions in terms of parabolic potentials, the set of irregular fluid/solid interface conditions are written in a matrix operator form as

$$\frac{\partial}{\partial r}\begin{pmatrix}A_f^I\\A_e^I\\B_r^I\\B_\theta^I\\B_z^I\end{pmatrix}=\begin{pmatrix}d_{11}&d_{12}&d_{13}&d_{14}&d_{15}\\d_{21}&d_{22}&d_{23}&d_{24}&d_{25}\\d_{31}&d_{32}&d_{33}&d_{34}&d_{35}\\d_{41}&d_{42}&d_{43}&d_{44}&d_{45}\\d_{51}&d_{52}&d_{53}&d_{54}&d_{55}\end{pmatrix}_{\mathrm{I}}\begin{pmatrix}A_f^I\\A_e^I\\B_r^I\\B_\theta^I\\B_z^I\end{pmatrix}, \tag{2.15}$$

where superscript **I** stands for irregular interface, and the elements d_{ij} of the above matrix considering far-field condition are given by

$$d_{11} \cong \left(\eta_r \frac{\partial}{\partial z}\right)^{-1}\left[-\eta_z \frac{\lambda_f k_f^2}{2\mu} - \eta_r i k_f \frac{\partial}{\partial z} - \eta_z \frac{\partial^2}{\partial z^2}\right], \quad d_{12} = \left(\eta_r \frac{\partial}{\partial z}\right)^{-1}\left[\eta_z \frac{\lambda k_L^2}{2\mu} e^{i(k_L - k_f)r}\right], \tag{2.16}$$

$$d_{13} = \left(\eta_r \frac{\partial}{\partial z}\right)^{-1}\left[-\eta_r \frac{1}{r^3} e^{i(k_T - k_f)r} \frac{\partial}{\partial \theta}\right], \quad d_{14} = \left(\eta_r \frac{\partial}{\partial z}\right)^{-1}\left[\eta_r \frac{k_T^2}{2} e^{i(k_T - k_f)r}\right], \quad d_{15} = 0,$$

$$L_e = \left\{\frac{2\eta_r^2 \eta_z}{r} - \eta_r\left(2+\eta_z^2\right)\frac{\partial}{\partial z} + \eta_z r \frac{\partial^2}{\partial z^2} + \frac{\eta_r^2 \eta_z}{r}\frac{\partial^2}{\partial \theta^2}\right\}\frac{\partial}{\partial z},$$

$$d_{21} = L_e^{-1} e^{i(k_f - k_L)r} \frac{\lambda_f k_f^2}{2\mu} \eta_r \eta_z \left[4\eta_r \frac{\partial}{\partial z} - 2\eta_z r \frac{\partial^2}{\partial z^2} + \frac{\eta_z}{r}\frac{\partial^2}{\partial \theta^2}\right],$$

$$d_{22} \cong L_e^{-1} \eta_r k_L \begin{Bmatrix} -\eta_r^2 \eta_z 2k_L \left(1+\frac{\lambda}{\mu}\right)\frac{\partial}{\partial z} - \eta_r \eta_z^2 \frac{\lambda k_L}{2\mu r}\frac{\partial^2}{\partial \theta^2} + \\ \eta_r \left[2i + \left(1+\frac{\lambda}{\mu}\right)\eta_z^2 k_L r\right]\frac{\partial^2}{\partial z^2} - \eta_r^2 \eta_z \frac{i}{r}\frac{\partial^3}{\partial \theta^2 \partial z} - \eta_z i r \frac{\partial^3}{\partial z^3} \end{Bmatrix}$$

$$d_{23} = L_e^{-1} e^{i(k_T - k_L)r} \frac{1}{r^2}\left\{\frac{2\eta_r}{r}\frac{\partial^2}{\partial \theta \partial z} - \eta_z \frac{\partial^3}{\partial \theta \partial z^2} + \frac{\eta_r^2 \eta_z}{r^2}\frac{\partial^3}{\partial \theta^3}\right\},$$

$$d_{24} \cong L_e^{-1} e^{i(k_T - k_L)r} \begin{Bmatrix} -\eta_r k_T^2 \frac{\partial}{\partial z} - \eta_r^2 \eta_z \frac{k_T^2}{2r}\frac{\partial^2}{\partial \theta^2} + \eta_z \frac{k_T^2}{2} r \frac{\partial^2}{\partial z^2} \\ -\eta_r\left(2+\eta_z^2\right)\frac{\partial^3}{\partial z^3} + \eta_r^2 \eta_z \frac{1}{r}\frac{\partial^4}{\partial \theta^2 \partial z^2} + \eta_z r \frac{\partial^4}{\partial z^4} \end{Bmatrix},$$

$$d_{25} = L_e^{-1} e^{i(k_T - k_L)r}\left\{-\eta_r^2 \eta_z k_T^2 \frac{\partial^2}{\partial \theta \partial z} + \frac{2\eta_r}{r}\frac{\partial^3}{\partial \theta \partial z^2} - \frac{\eta_r^2 \eta_z}{r^2}\frac{\partial^4}{\partial \theta^3 \partial z} - \eta_z \frac{\partial^4}{\partial \theta \partial z^3}\right\}, \tag{2.17}$$

$$d_{31} = 0, \quad d_{32} = 0, \quad d_{33} \cong -ik_T, \quad d_{34} = -\frac{\partial}{\partial \theta}, \quad d_{35} = -r\frac{\partial}{\partial z}, \tag{2.18}$$

$$d_{41} = \frac{e^{i(k_f - k_T)r}}{L_e}\left(-\frac{\lambda_f k_f^2}{2\mu}\right)\begin{bmatrix} \eta_r^2 \eta_z \frac{2}{r} + \eta_r\left(2-5\eta_z^2\right)\frac{\partial}{\partial z} + \eta_r^2 \eta_z \frac{2}{r}\frac{\partial^2}{\partial \theta^2} \\ +\eta_z\left(\eta_z^2 - \eta_r^2\right) r \frac{\partial^2}{\partial z^2} \end{bmatrix},$$

$$d_{42} \cong \frac{e^{i(k_L - k_T)r}}{L_e}\begin{Bmatrix} \frac{\eta_r^2 \eta_z \lambda k_L^2}{\mu r} + 2\eta_r k_L^2\left[\frac{\left(2-5\eta_z^2\right)\lambda}{4\mu} + \eta_r^2\right]\frac{\partial}{\partial z} + \frac{\eta_r^2 \eta_z \lambda k_L^2}{\mu r}\frac{\partial^2}{\partial \theta^2} \\ -\frac{\eta_r^2 \eta_z}{r}\frac{\partial^4}{\partial \theta^2 \partial z^2} + \eta_z k_L^2 r\left[\left(\eta_z^2 - \eta_r^2\right)\frac{\lambda}{2\mu} - \eta_r^2\right]\frac{\partial^2}{\partial z^2} \\ +\eta_r\left(2+\eta_z^2\right)\frac{\partial^3}{\partial z^3} - \eta_z r \frac{\partial^4}{\partial z^4} \end{Bmatrix},$$

$$
\begin{aligned}
d_{43} &= \frac{1}{L_e r}\left\{\begin{array}{l} -\eta_r^3\frac{2}{r^3}\frac{\partial}{\partial\theta}+\eta_r^2\eta_z\frac{3}{r^2}\frac{\partial^2}{\partial\theta\partial z}-\eta_r^3\frac{2}{r^3}\frac{\partial^3}{\partial\theta^3}-\eta_r\left(2+\eta_z^2\right)\frac{1}{r}\frac{\partial^3}{\partial\theta\partial z^2} \\ +\eta_r^2\eta_z\frac{1}{r^2}\frac{\partial^4}{\partial\theta^3\partial z}+\eta_z\frac{\partial^4}{\partial\theta\partial z^3} \end{array}\right\}, \\
d_{44} &\cong \frac{k_T}{L_e}\left\{\begin{array}{l} \eta_r^3\frac{k_T}{r}-\eta_r^2\eta_z\frac{k_T}{2}\frac{\partial}{\partial z}+\eta_r^3\frac{k_T}{r}\frac{\partial^2}{\partial\theta^2}+\eta_r\left(2+\eta_z^2\right)i\frac{\partial^2}{\partial z^2} \\ -\eta_r^2\eta_z i\frac{1}{r}\frac{\partial^3}{\partial\theta^2\partial z}-\eta_z ir\frac{\partial^3}{\partial z^3} \end{array}\right\}, \\
d_{45} &\cong \frac{\eta_r^2}{L_e}\left\{\eta_r k_T^2\frac{\partial^2}{\partial\theta\partial z}+\eta_z\frac{1}{r}\frac{\partial^3}{\partial\theta\partial z^2}\right\},
\end{aligned}
\tag{2.19}
$$

and

$$
\begin{aligned}
d_{51} &= L_e^{-1}e^{i(k_f-k_T)r}\frac{\lambda_f k_f^2}{2\mu}\eta_z\left[\eta_r\eta_z\frac{1}{r}\frac{\partial}{\partial\theta}+\left(2\eta_z^2-3\right)\frac{\partial^2}{\partial\theta\partial z}\right], \\
d_{52} &\cong L_e^{-1}e^{i(k_L-k_T)r}\left\{\begin{array}{l} -\eta_r\eta_z^2\frac{\lambda k_L^2}{2\mu}\frac{1}{r}\frac{\partial}{\partial\theta}+\eta_z k_L^2\left[\left(\frac{3}{2}-\eta_z^2\right)\frac{\lambda}{\mu}+\eta_r^2\right]\frac{\partial^2}{\partial\theta\partial z} \\ -\eta_r\left(2+\eta_z^2\right)\frac{1}{r}\frac{\partial^3}{\partial\theta\partial z^2}+\eta_z\frac{\partial^4}{\partial\theta\partial z^3}+\eta_r^2\eta_z\frac{1}{r^2}\frac{\partial^4}{\partial\theta^3\partial z} \end{array}\right\}, \\
d_{53} &= L_e^{-1}\left\{\begin{array}{l} \frac{\eta_r^2\eta_z}{r^4}\frac{\partial^2}{\partial\theta^2}+\frac{2\eta_r^2\eta_z}{r^2}\frac{\partial^2}{\partial z^2}-\frac{2\eta_r}{r^3}\frac{\partial^3}{\partial\theta^2\partial z}-\frac{\eta_r\left(2+\eta_z^2\right)}{r}\frac{\partial^3}{\partial z^3} \\ +\frac{\eta_r^2\eta_z}{r^2}\frac{\partial^4}{\partial\theta^2\partial z^2}+\eta_z\frac{\partial^4}{\partial z^4} \end{array}\right\}, \\
d_{54} &= L_e^{-1}\eta_r k_T^2\left\{-\eta_r\eta_z\frac{1}{2r}\frac{\partial}{\partial\theta}+\frac{\partial^2}{\partial\theta\partial z}\right\}, \\
d_{55} &\cong L_e^{-1}k_T\left\{-\eta_r^2\eta_z k_T\frac{\partial}{\partial z}+\eta_r k_T r\frac{\partial^2}{\partial z^2}-\eta_r^2\eta_z i\frac{1}{r}\frac{\partial^3}{\partial\theta^2\partial z}-\eta_z ir\frac{\partial^3}{\partial z^3}\right\}.
\end{aligned}
\tag{2.20}
$$

2.3 Representative Coupled 3D Wave Equations in PE system form

Let $\mathbf{V}=\left(A_f, A_f^I, A_e^I, B_r^I, B_\theta^I, B_z^I, A_e, B_r, B_\theta, B_z\right)^T$. The superscript T stands for the transpose. Combining the parabolic elastic wave equations in operator matrix form (2.5), the parabolic fluid wave equation in operator matrix form (2.7), and the parabolic irregular interface vector equations in operator matrix form (2.15) gives the representative coupled 3D wave equations in the following operator matrix form:

$$
\frac{\partial\mathbf{V}}{\partial r}=\underline{\mathbf{M}}\mathbf{V}+\underline{\mathbf{G}}, \tag{2.21}
$$

where

$$\mathbf{M}=\begin{Bmatrix} \begin{bmatrix} & & \\ & \mathrm{A}_f & \\ & & \end{bmatrix} & \mathbf{0} & \mathbf{0} \\ \mathbf{0} & \begin{bmatrix} d_{11} & d_{12} & d_{13} & d_{14} & d_{15} \\ d_{21} & d_{22} & d_{23} & d_{24} & d_{25} \\ d_{31} & d_{32} & d_{33} & d_{34} & d_{35} \\ d_{41} & d_{42} & d_{43} & d_{44} & d_{45} \\ d_{51} & d_{52} & d_{53} & d_{54} & d_{55} \end{bmatrix} & \mathbf{0} \\ \mathbf{0} & \mathbf{0} & \begin{bmatrix} \mathrm{A}_L & 0 & 0 & 0 \\ 0 & \mathrm{A}_T & 0 & \mathrm{B}_T\left(-\frac{\partial}{\partial z}\right) \\ 0 & \mathrm{B}_T\left(-\frac{1}{r^3}\frac{\partial}{\partial \theta}\right) & \mathrm{A}_T & 0 \\ 0 & 0 & 0 & \mathrm{A}_T \end{bmatrix} \end{Bmatrix}. \tag{2.22}$$

The vector $\underline{\mathbf{G}}$ is a function related to boundary conditions. The operators d_{ij} couple the elements between the interface and the fluid medium as well as the elastic medium.

After a PE system is formulated in operators form, the next stage is to transform Eq. (2.21) into a numerical model. As the operator matrix $\mathbf{M}$ is discretized and Eq. (2.21) becomes a system of difference equations, the coupling between medium and interface will be obviously shown by visualizing the discretized coefficients matrix $\mathbf{M}$.

3 Numerical Modeling

This section is focused on transforming the theoretical PE expression into a numerical model consisting of three parts: theoretical development, computational aspects, and the development of the computer code.

3.1 Scheme Development

It is expected that for a coupled problem in heterogeneous media invested in this paper, the computational scheme will be based on an ODE, or split-step concept.

3.1.1 Marching Scheme

Assume that coupled wave PE system (2.21) has the discrete local solution as

$$\mathbf{V}(r+\Delta r)=e^{\Delta r\mathbf{M}}\mathbf{V}(r)+\left(e^{\Delta r\mathbf{M}}-\mathbf{I}\right)\mathbf{M}^{-1}\mathbf{G}(r). \tag{3.1}$$

By direct replacing the exponential matrix in Eq. (3.1) by (1,1) Padé approximant, the result is obtained as the well known Crank-Nicolson scheme:

$$\left(\mathbf{I}-\tfrac{1}{2}\Delta r\mathbf{M}\right)\mathbf{V}^{n+1}=\left(\mathbf{I}+\tfrac{1}{2}\Delta r\mathbf{M}\right)\mathbf{V}^{n}+\Delta r\mathbf{G}^{n}. \tag{3.2}$$

Equation (3.2) is chosen to be the essential marching scheme of the proposed numerical solution in this paper.

If (2,2) Padé approximant is applied to the exponential matrix in Eq. (3.1), the following higher order scheme is obtained

$$\left[\mathbf{I}-\tfrac{1}{2}\Delta r\mathbf{M}+\frac{1}{12}(\Delta r\mathbf{M})^2\right]\mathbf{V}^{n+1}=\left[\mathbf{I}+\tfrac{1}{2}\Delta r\mathbf{M}+\frac{1}{12}(\Delta r\mathbf{M})^2\right]\mathbf{V}^{n}+\Delta r\mathbf{G}^{n}. \tag{3.3}$$

Note that higher, such as (3,3), Padé approximants will make the coefficient of $\mathbf{G}^n$ not simple as Δr only.

3.1.2 Numerical ODE Formulation for Wave and Interface Equations

To obtain the coefficients matrix of numerical scheme, all the derivatives are expressed in finite difference formulation. The complete derivation and results are very lengthy and therefore referred to the first author's Ph.D. dissertation [16]. Here only parts of them are presented as examples.

For elastic and fluid wave equations, the operators containing derivatives are in a square root. Therefore it is necessary to have an approximation for the square root. The square root approximation can lead to computational phase errors. These phase errors have the physical meaning of limitation in propagation angle [8, 10]. Higher order approximations reduce the phase errors and result in wide-angle models [9]. This issue has been broadly investigated and many wide-angle models were developed in the past two decades. It has been proved that narrow-angle formulation ($\leq 23^\circ$) is not adequate for sound propagation in shallow water and a wide-angle model must be used instead [7, 8, 10]. Nevertheless, most of those models referred to be wide-angle in depth because they are only considering 2-D problems and thus the azimuthal angle is not well discussed until recent years.

Among numbers of square root approximations, a second order approximation [7] is written as

$$\sqrt{1+Z}\cong 1+\frac{1}{2}Z-\frac{1}{8}Z^2+O\left(Z^3\right). \tag{3.4}$$

For parabolic wave equations, the operator Z is

$$Z_{i=f,L,T}=\frac{1}{k_i^2}\left(\frac{\partial^2}{\partial z^2}+\frac{1}{r^2}\frac{\partial^2}{\partial\theta^2}\right). \tag{3.5}$$

In the above, f,L,T represent of fluid, longitudinal, and transverse elastic quantities, respectively. If second order is considered in depth where as only first order is considered in azimuth, then the square root approximation is

$$\sqrt{1+\frac{1}{k_i^2}\left(\frac{\partial^2}{\partial z^2}+\frac{1}{r^2}\frac{\partial^2}{\partial\theta^2}\right)}\cong 1+\frac{1}{2k_i^2}\frac{\partial^2}{\partial z^2}-\frac{1}{8k_i^4}\frac{\partial^4}{\partial z^4}+\frac{1}{2k_i^2r^2}\frac{\partial^2}{\partial\theta^2}. \tag{3.6}$$

The above expression is also adopted in Ref. [5]. For consistency and higher accuracy, all the difference formulae are chosen of the second order.

As for $\left(\sqrt{1+Z}\right)^{-1}$ in parabolic elastic wave equations for B_r and B_θ, it can be approximated via a Taylor series expansion with the polynomial functions

$$\left[\sqrt{1+\frac{1}{k_i^2}\left(\frac{\partial^2}{\partial z^2}+\frac{1}{r^2}\frac{\partial^2}{\partial\theta^2}\right)}\right]^{-1}\cong 1-\frac{1}{2k_i^2}\frac{\partial^2}{\partial z^2}+\frac{3}{8k_i^4}\frac{\partial^4}{\partial z^4}-\frac{1}{2k_i^2r^2}\frac{\partial^2}{\partial\theta^2}. \tag{3.7}$$

With Eqs. (3.6) and (3.7), the parabolic elastic and fluid wave equations can be explicitly discretized. Take fluid wave equation (2.7) as example:

$$\frac{\partial A_{f(i,j)}}{\partial r} = \alpha_{f2}\left[A_{f(i+2,j)} + A_{f(i-2,j)}\right] + \alpha_{fz1}\left[A_{f(i+1,j)} + A_{f(i-1,j)}\right] + \alpha_{f\theta 1}\left[A_{f(i,j+1)} + A_{f(i,j-1)}\right] + \alpha_f A_{f(i,j)}, \tag{3.8}$$

where

$$\alpha_{f2} = -\frac{ik_f}{8\left(k_f\Delta z\right)^4}, \alpha_{fz1} = \frac{ik_f}{2\left(k_f\Delta z\right)^2} + \frac{ik_f}{2\left(k_f\Delta z\right)^4},$$
$$\alpha_{f\theta 1} = \frac{ik_f}{2\left(k_f r\Delta\theta\right)^2}, \alpha_f = -\left(\frac{ik_f}{\left(k_f\Delta z\right)^2} + \frac{3ik_f}{4\left(k_f\Delta z\right)^4} + \frac{ik_f}{\left(k_f r\Delta\theta\right)^2}\right). \tag{3.9}$$

The subscripts i, j represent the i th grid point in depth, and j th grid point in azimuth. Note that if $\Delta\theta$ is chosen so large as $1/\Delta\theta$ approaches zero, the equations reduce to two-dimensional case.

In equation for B_r, the operator coefficient of B_z is approximated using Eq. (3.7) and resulting in

$$\frac{1}{ik_T\sqrt{1+L_T}}\left(-\frac{\partial}{\partial z}\right) = \frac{i}{k_T}\left(\frac{\partial}{\partial z} - \frac{1}{2k_T^2}\frac{\partial^3}{\partial z^3} + \frac{3}{8k_T^4}\frac{\partial^5}{\partial z^5} - \frac{1}{2k_T^2 r^2}\frac{\partial^3}{\partial\theta^2\partial z}\right). \tag{3.10}$$

In equation for B_θ, the operator coefficient of B_r is also approximated using Eq. (3.7) and resulting in

$$\frac{1}{ik_T\sqrt{1+L_T}}\left(-\frac{1}{r^3}\frac{\partial}{\partial\theta}\right) = \frac{i}{r^3 k_T}\left(\frac{\partial}{\partial\theta} - \frac{1}{2k_T^2}\frac{\partial^3}{\partial\theta\partial z^2} + \frac{3}{8k_T^4}\frac{\partial^5}{\partial\theta\partial z^4} - \frac{1}{2k_T^2 r^2}\frac{\partial^3}{\partial\theta^3}\right). \tag{3.11}$$

As a summary, with the square root approximations and proper discretization, the numerical ODE formulations for elastic and fluid wave equations like Eq. (3.8) and the interface equations can be obtained. The complete results are referred to the first author's Ph.D. dissertation [16] and not shown here. Results for wave equations in Ref. [5] are similar except for its equation of B_r where an error occurs in their derivation of wave equation for B_r.

3.2 Computational Aspects

In order to develop the computer code, a number of computational aspects have to be taken into consideration.

For simplicity, taking a horizontal interface problem as an example, Fig. 3.1 schematically shows computation grids and settings. As shown in Fig. 3.1, the upper boundary which usually refers to the ocean surface is assumed to be flat and pressure released

$$A_f\big|_{z=0} = 0. \tag{3.12}$$

The lower boundary denoted as rigid bottom is assumed to be flat and force the first derivatives with respect to depth of all quantities to be zero

$$\frac{\partial}{\partial z} Q \Big|_{z=H_b} = 0, \tag{3.13}$$

resulting to be a total reflecting boundary. The bottom boundary can also be set to zero for simplicity.

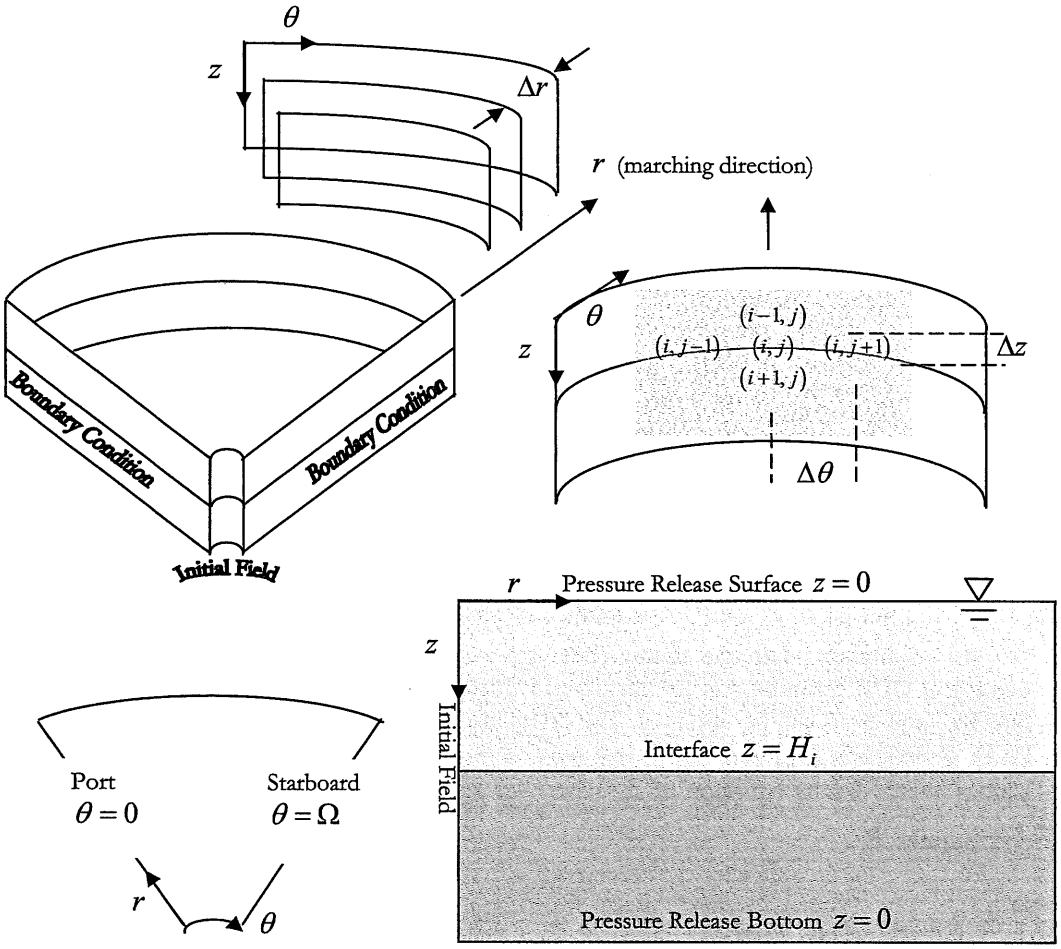

Fig. 3.1 Schematic of computation grids and settings

In order not to use nonphysical points outside the boundaries in difference equations for the grid points near boundaries, forward/backward difference formulas are applied. For example, at $z = \Delta z$ the second order forward difference formula of the forth depth derivative, $\left.\frac{\partial^4 p}{\partial z^4}\right|_{z=\Delta z}$ is given as

$$\frac{2p_0 - 9p_1 + 16p_2 - 14p_3 + 6p_4 - p_5}{(\Delta z)^4}, \tag{3.14}$$

where p_0 vanishes if pressure release condition is considered. This formula induces inconsistency error which will be shown in a test case in next section.

Nevertheless, the mirror effect, $p_{-i} = -p_i$, at pressure release boundaries, $p_0 = 0$, can be applied so that central difference formula can still be applicable without using nonphysical points as Fig. 3.2 shows. Therefore the second order central difference formula of the forth depth derivative, $\left.\frac{\partial^4 p}{\partial z^4}\right|_{z=\Delta z}$ is given as

$$\frac{p_{-1} - 4p_0 + 6p_1 - 4p_2 + p_3}{(\Delta z)^4} = \frac{-p_1 + 6p_1 - 4p_2 + p_3}{(\Delta z)^4} = \frac{5p_1 - 4p_2 + p_3}{(\Delta z)^4}. \tag{3.15}$$

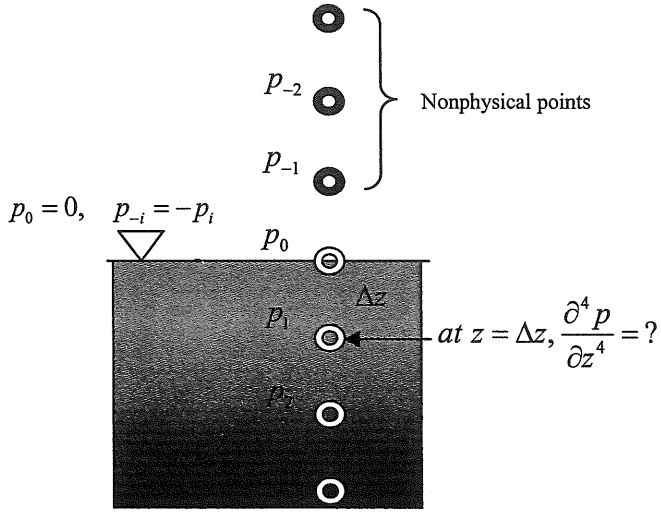

Fig. 3.2 Schematic of pressure release boundary in discrete space.

Comparing Eqs. (3.14) and (3.15), it can be noted that considering mirror effect at pressure release boundaries not only maintains the consistency of using central difference formulas but also reduces the number of grid points from five to three at $z = \Delta z$.

For the port/starboard sidewall boundaries, they are not pressure released or rigid under most circumstances except for numerical tests. In realistic situations, they are not known and have to be computed and provided as boundary conditions of Dirichlet type

$$Q|_{\theta=0,\Omega} = f_{0,\Omega}. \tag{3.16}$$

2D $(r-z)$ solutions may be the most straightforward answers provided for sidewall boundaries.

A computer code is developed to implement the marching implicit scheme (3.2). However, it must be mentioned that the mathematic and numerical development of the proposed model does not contain the density variation and other capability enhancement, the computer code is basically a research code. It still needs some efforts to turn this code into a practically working code like other well known models, say, FOR3D.

The geometry of propagation has been presented in Fig. 3.1. The data structure should be particularly noticed since this model deals with a heterogeneous problem. That is, at a

single grid point, there are more than one unknown quantities. Each field quantities $A_f, A_e, B_r, B_\theta, B_z$ is stored in separate matrices at the beginning and in its final form. However, during the calculation stage, solving the unknowns requires these field quantities to be organized as a single vector at each range step. The coefficient matrix corresponding to this unknown vector is thus constructed as the following figure shows along with the structure of the unknown vector. The figure shows an example of 9 azimuth sections (side-wall boundaries excluded). Blue dots represent nonzero elements which are the coefficients of the difference equations. It can be seen that the matrix is formed as a band-matrix. Dark lines indicate different azimuth sections whereas the red dashed lines showing the five interface equations between the fluid and the elastic wave equations which are colored with light blue and olive boxes, respectively. The unknown vector is a column shown at right hand side of the coefficient matrix.

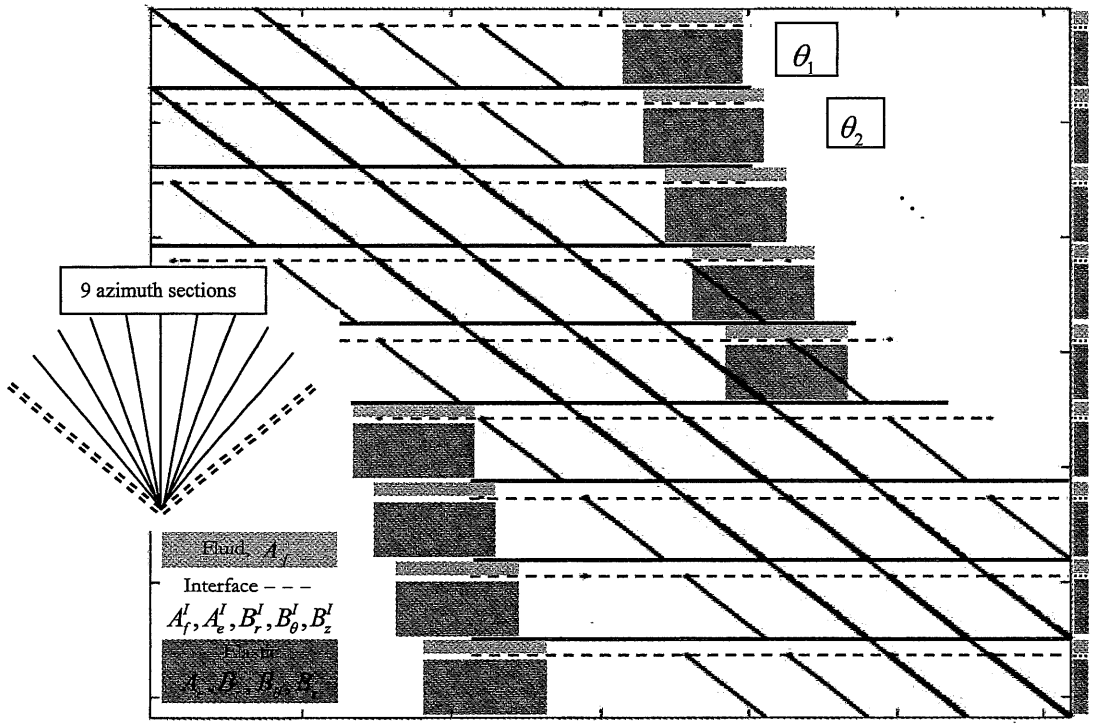

Fig. 3.3 Data structure of the coefficient matrix and unknown vector.

4 Model Appraisal

In this section, several test cases are investigated to validate the model and also to show the model's application and ability. Exact solutions to the coupled 3D wave propagation problems are practically unachievable due to complexities in environment and boundaries. To validate models claiming to solve these problems is therefore limited.

In the following, several examples will be presented to start from the simplest two-dimensional range-independent problem for waves in fluid only, and finally to the coupled 3D wave propagation model with irregular interface.

4.1 2D Fluid Waves in Range-Independent Environment

Being the first step to validate the model, this example is focused on testing the numerical marching scheme Eq. **(3.2)**. Also the effect of considering the mirror effect on pressure release boundaries as prescribed in previous section is presented.

Considering a two-dimensional (r,z) plane, the upper and lower boundaries are both flat and pressure-released, and the medium in between the two boundaries is pure fluid only without any energy absorption. The environment is totally range-independent.

Numerical ODE formulation for the 2D fluid wave equation can be obtained by applying the square root approximation **(3.4)** and **(3.5)** resulting similar to Eq. **(3.6)** as

$$\frac{\partial A_f}{\partial r} = ik_f\left(\frac{1}{2k_f^2}\frac{\partial^2}{\partial z^2} - \frac{1}{8k_f^4}\frac{\partial^4}{\partial z^4}\right)A_f. \tag{4.1}$$

To find the general solution to the above equation, one can use the method of separation of variables given the initial condition $A_f(0,z) = \sin\left(\frac{\pi z}{H}\right)$ and obtain

$$A_f = \exp\left\{-ir\left[\frac{(\pi/H)^2}{2k_f} + \frac{(\pi/H)^4}{8k_f^3}\right]\right\}\cdot\sin\left(\frac{\pi z}{H}\right). \tag{4.2}$$

Using the presented numerical model, a banded matrix is formed to solve the problem with computation parameters set as $\Delta z = 0.1\lambda_f, \Delta r = 3\lambda_f$, where sound speed c is 1500 m/s, sound frequency f is 200 Hz, water depth H is 60 m, wavelength λ_f is 7.5 m. Figure 4.1 compares the absolute value of computed solutions using (1,1)/(2,2) Padé scheme and sided/central difference near boundaries for range 0 - 12 km. It can be clearly seen that errors accumulate from the upper and lower boundaries if mirror effect is not considered and sided difference is applied. Also higher order scheme, such as (2,2) Padé scheme, is more sensitive to such errors from boundaries. However, if mirror effect is taken into account, then the errors are removed and (2,2) Padé scheme produces better results as it is expected.

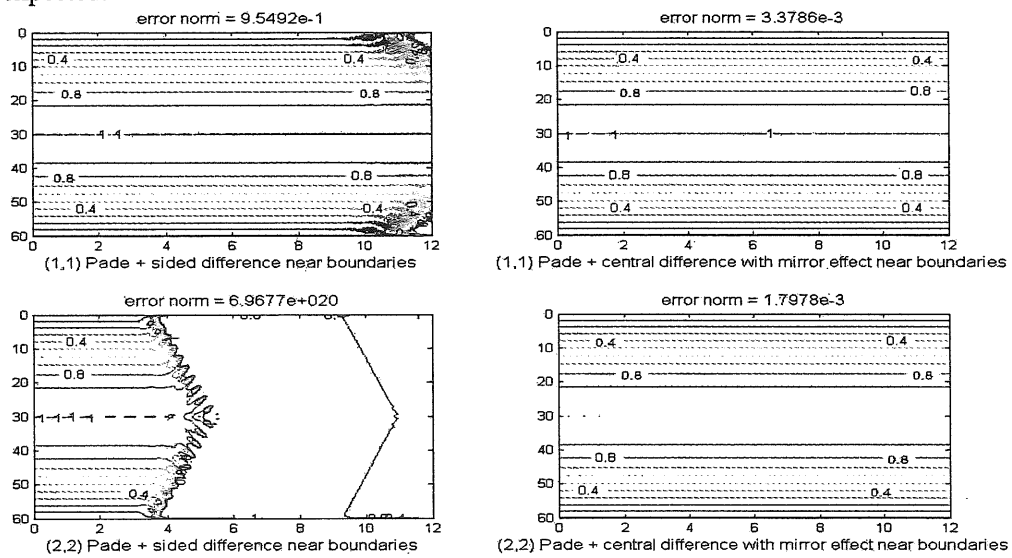

Fig. 4.1 Comparison between the computed solutions using (1,1)/(2,2) Padé scheme and sided/central difference near boundaries.

By this test case, the marching scheme using (1,1)/(2,2) Padé approximations are validated. The improvement of considering mirror effect near pressure release boundaries is also presented. This suggests the consideration of mirror effect in all computations when pressure release boundaries occur.

4.2 2D Elastic Waves in Range-Independent Environment

The elastic wave governing equations are coupled for 3D propagation as two individual systems, $\{A_e\}$ and $\{B_r, B_\theta, B_z\}$. For 2D propagation, θ-derivatives are dropped so that B_r is uncoupled from the equation of B_θ, therefore the governing equations are further uncoupled into three independent sets, $\{A_e\}$, $\{B_\theta\}$, and $\{B_r, B_z\}$. Provided there is no coupling mechanism on boundaries, 2D elastic waves problem can be resolved by separately finding the solutions of the three systems.

Given the same flat and pressure-released upper and lower boundaries as in the previous case for fluid wave problem, since equations of $\{A_e\}$ and $\{B_\theta\}$ are of the same form as that of $\{A_f\}$, similar analytic solutions and results presented in the previous case can be obtained. Hence here we will focus on the two-variable coupled system, $\{B_r, B_z\}$. Note that under these pressure-released boundary conditions, if B_z is initially unexcited, i.e., $B_z|_{r=0} = 0$, then B_z will be decoupled from the equation of B_r. Therefore the problem is reduced to the same form of $\{A_f\}$, and the whole B_z field will be completely silent, thus the equation of B_z turns out to be trivial and its calculation may be saved.

After applying square root approximations **(3.6)** and **(3.7)**, the two-variable coupled system, $\{B_r, B_z\}$ writes

$$\begin{aligned}
\frac{\partial B_z}{\partial r} &= ik_T\left(\frac{1}{2k_T^2}\frac{\partial^2}{\partial z^2} - \frac{1}{8k_T^4}\frac{\partial^4}{\partial z^4}\right)B_z, \\
\frac{\partial B_r}{\partial r} &= ik_T\left(\frac{1}{2k_T^2}\frac{\partial^2}{\partial z^2} - \frac{1}{8k_T^4}\frac{\partial^4}{\partial z^4}\right)B_r + \frac{i}{k_T}\left(\frac{\partial}{\partial z} - \frac{1}{2k_T^2}\frac{\partial^3}{\partial z^3} + \frac{3}{8k_T^4}\frac{\partial^5}{\partial z^5}\right)B_z.
\end{aligned} \tag{4.3}$$

As before, the analytic solution to Eq. (4.3) is desired. The strategy to solve Eq. (4.3) is summarized as two steps. The first step is to solve the parabolic equation for B_z, and this is followed by solving the parabolic equation for B_r with the part containing derivatives of B_z known as the inhomogeneous source term.

By the method of separation of variables, B_z can be derived in the form of

$$B_z = \exp\left(-ik_T\varsigma^2 r\right)\left[C_1\underline{\exp\left(\ell_1 z\right)} + C_2\underline{\exp\left(-\ell_1 z\right)} + C_3\underline{\sin\left(\ell_2 z\right)} + C_4\underline{\cos\left(\ell_2 z\right)}\right], \tag{4.4}$$

where the functions with underline are the eigenfunctions, and ℓ_1, ℓ_2 are related to the eigenvalues as

$$\ell_{1,2} = \sqrt{2}k_T\sqrt{\sqrt{1+2\varsigma^2}\pm 1}. \tag{4.5}$$

Note that the given boundary conditions $B_z(r,0)=B_z(r,H)=0$ are not sufficient to define the coefficients C_i. However, with proper initial conditions input, the coefficients can be determined. It is obvious that $\sin\left(\frac{n\pi}{H}z\right)$ for any integer n can satisfy the zero boundary conditions. Further more, it is of the same form with one of the eigenfunctions, $\sin(\ell_2 z)$. Therefore, if the initial filed is given as $C_0\sin\left(\frac{n\pi}{H}z\right)$, where C_0 is a constant, then

$$B_z(0,z) = C_1\exp(\ell_1 z)+C_2\exp(-\ell_1 z)+C_3\sin(\ell_2 z)+C_4\cos(\ell_2 z) = C_0\sin\left(\frac{n\pi}{H}z\right), \tag{4.6}$$

the coefficients in Eq. (4.4) can be determined as $C_1 = C_2 = C_4 = 0$, and $C_3 = C_0$ a known constant. Also it leads to $\ell_{2,n} = \frac{n\pi}{H}$, so that the eigenvalues are given as

$$\varsigma_n^2 = \frac{1}{2}\left(\frac{n\pi}{k_T H}\right)^2 + \frac{1}{8}\left(\frac{n\pi}{k_T H}\right)^4, \tag{4.7}$$

and thus the analytic solutions to B_z is then written as

$$B_z = C_0\exp\left\{-ik_T\left[\frac{1}{2}\left(\frac{n\pi}{k_T H}\right)^2 + \frac{1}{8}\left(\frac{n\pi}{k_T H}\right)^4\right]r\right\}\sin\left(\frac{n\pi}{H}z\right). \tag{4.8}$$

The analytic solution to A_f in the previous case can be verified by the above equation as well where $n=1, C_0=1$.

Next step is to substitute Eq. (4.8) into Eq. (4.3) to solve the equation for B_r. After the substitution, it reduces to

$$\begin{aligned}\frac{\partial B_r}{\partial r} &= ik_T\left(\frac{1}{2k_T^2}\frac{\partial^2}{\partial z^2} - \frac{1}{8k_T^4}\frac{\partial^4}{\partial z^4}\right)B_r \\ &+C_0 i\exp\left(-ik_T\varsigma_n^2 r\right)\left[\frac{n\pi}{k_T H} + \frac{1}{2}\left(\frac{n\pi}{k_T H}\right)^3 + \frac{3}{8}\left(\frac{n\pi}{k_T H}\right)^5\right]\cos\left(\frac{n\pi}{H}z\right).\end{aligned} \tag{4.9}$$

Equation (4.9) is an inhomogeneous PDE which can be solved by eigenfunction expansion method [13]. If $n=2, C_0=1$ is chosen to have the initial condition for B_z being $B_z(r,0) = \sin\left(\frac{2\pi}{H}z\right)$, and a static initial condition for B_r, i.e., $B_r(r,0)=0$, the solution to Eq. (4.9) is obtained as

$$B_r = \sum_{n=1,3,5,\ldots}^{\infty}\frac{4nA_0\left(e^{-A_2 r}-e^{-A_n r}\right)}{\pi\left(n^2-4\right)\left(A_n-A_2\right)}\sin\left(\frac{n\pi}{H}z\right), \tag{4.10}$$

where

$$A_0 = i\left[2\left(\frac{\pi}{k_T H}\right)+4\left(\frac{\pi}{k_T H}\right)^3+12\left(\frac{\pi}{k_T H}\right)^5\right], A_2 = 2ik_T\left[\left(\frac{\pi}{k_T H}\right)^2+\left(\frac{\pi}{k_T H}\right)^4\right], \quad (4.11)$$

$$A_n = ik_T\left[\frac{1}{2}\left(\frac{n\pi}{k_T H}\right)^2+\frac{1}{8}\left(\frac{n\pi}{k_T H}\right)^4\right], n = 1,3,5,\cdots.$$

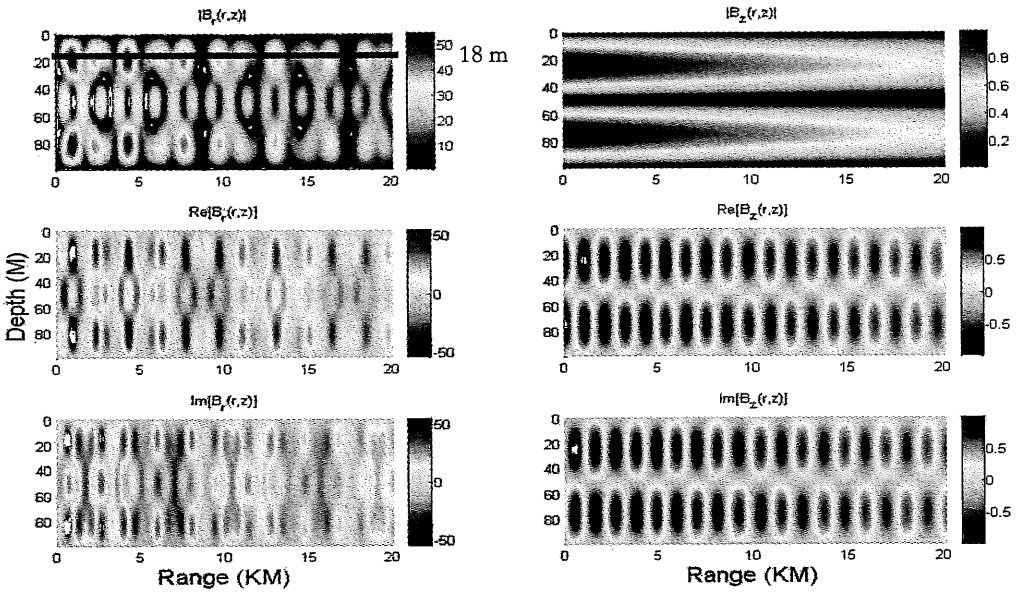

Fig. 4.2 Absolute value, real part, and imaginary part of the numerical solutions to 2D elastic wave problem (4.3).

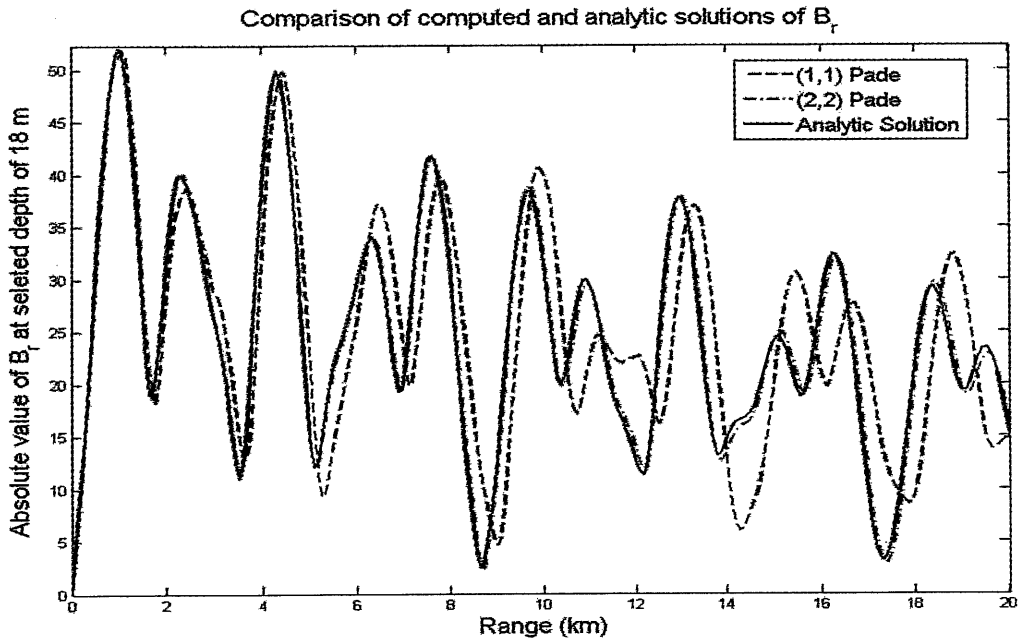

Fig. 4.3 Comparison of (1,1)/(2,2) Padé schemes and analytic solutions of B_r at depth of 18 m.

Given the depth $H = 99$ m, wave frequency $f = 100$ Hz, transverse wave speed $c_T = 900$ m/s, the numerical solutions of B_z and B_r are plotted in Fig. 4.2 for range 0 – 20 km considering the absorption coefficient being 0.5 dB per wavelength. Setting the computational parameters $\Delta z = 0.2\lambda_T$ and $\Delta r = 8\lambda_T$, the numerical results of B_r agree well with the analytic solution at selected depth of 18 m shown in Fig. 4.3. However, (1,1) Padé scheme does not provide as good prediction as (2,2) Padé scheme for this case.

4.3 Coupled 2D Waves with Irregular Interface

In this test case, at first a down-slope wedge is considered then an up-slope wedge. Both slope ratios are 1:20, or about ±2.86°, and the water depth at source location is 200 m. A Greene's source is placed at depth of 30 m, the computation parameters are set as $\Delta z = 0.18m, \Delta r = 3.6m$, and the absorption coefficient being 0.5 dB per wavelength. Figure 4.4 shows the computed solutions in water column, $|A_f|$, in the upper two plots.

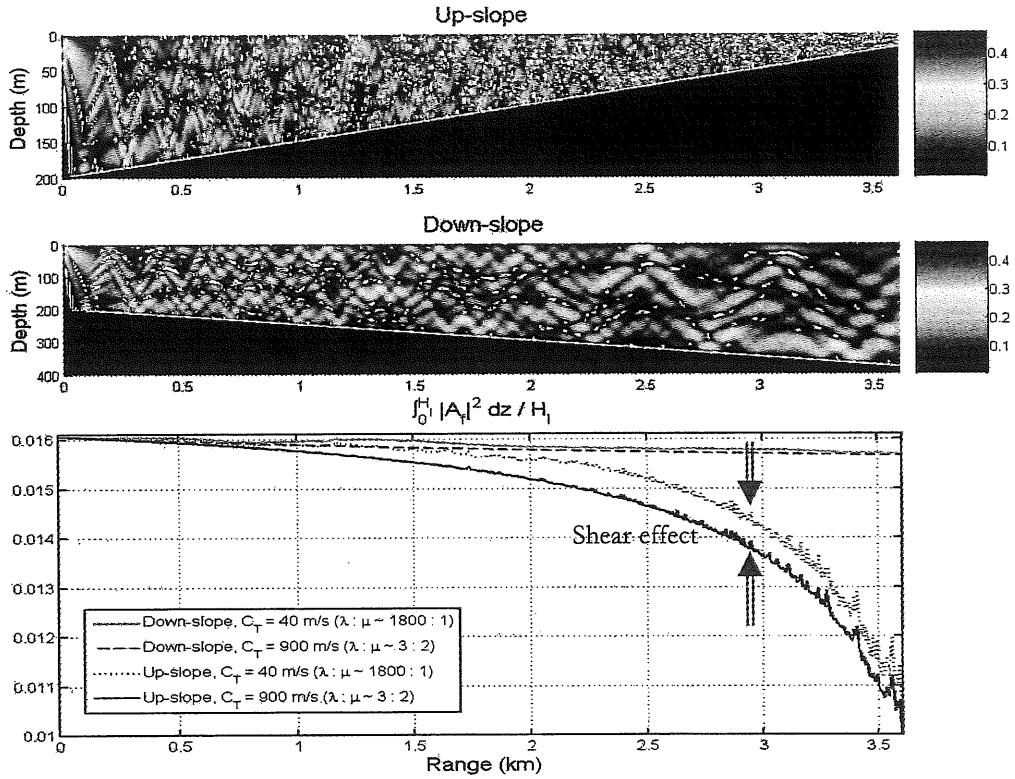

Fig. 4.4 Comparison between the calculated results of up/down-slope wedge with low/high shear wave speed.

The lower plot compares the depth averaged energy along the propagation range for four difference situations. The green solid line represents the result calculated in down-slope wedge with very low shear wave speed (c_T = 40 m/s) comparing to the red dashed line where the shear wave speed is 900 m/s. These two line does not differ too much, i.e., shear effect is not obvious in down-slope wedge. In up-slope wedge, energy in water column is expected apparently decreasing due to more interaction between wave and bottom as shown in the figure. The blue dotted line represents the result calculated in

up-slope wedge with shear wave speed being 40 m/s whereas the black solid line is the case with $c_T = 900$ m/s. It can be seen from the figure that there is noticeable difference due to shear effect for up-slope wedge. More energy of water column is transferred into bottom as shear wave.

4.4 Coupled 3D Waves with Irregular Interface

It has to be noticed as mentioned before that the analytic solutions to such problems are inaccessible.

For simplicity, the upper and lower boundary conditions are pressure released boundaries, and the two side-wall boundary conditions are zeros as well. Given the environment setting being the same as before except for total depth of $H = 70$ m and a range-dependent bathymetry $H_I(r)$. For sound frequency of 25 Hz, the initial field is placed at $r_0 = 1082.3$ m to satisfy far-field approximation $k_i r \geq 100$, $i = f, L, T$. The computational parameters are set as: $\Delta r = 0.4\lambda_T = 14.4$ m, $\Delta\theta = 0.5°$, and $\Delta z = 0.015\lambda_T = 0.54$ m. It must be noted that Δz is chosen so small to have accurate solutions because of the interface effect. Starting from r_0, the initial field is propagated 150 m which is about 10 range steps, and the computation span is 20 degrees which consists 21 sections including two side-wall boundaries. The bathymetry is defined as $H_I(r_0) = 35, H_I(r_0 + 50) = 36, H_I(r_0 + 100) = 34$, and $H_I(r_0 + 150) = 37$, as shown in Fig. 4.5. It must be emphasized that the bathymetry is given of axial symmetry to be consistent with the irregular interface defined and shown in Fig. 2.1.

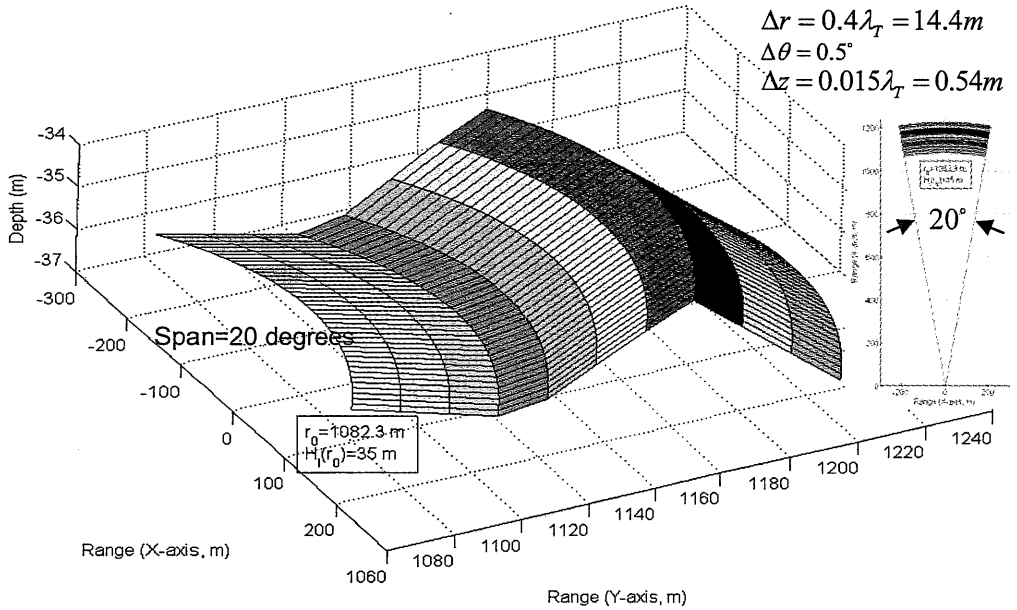

Fig. 4.5 Schematic of 3D bathymetry and other computational settings.

To have a 3D initial field instead of an Nx2D field, all the field is initially static except for $A_f(r_0, \theta = 0, z)$ is excited by a normalized sinc function. The calculated results are plotted in Figs. 4.6 – 4.7 where the absolute values of $A_f, A_e, B_r, B_\theta, B_z$ are shown. The

solutions are selected from three specified ranges: the next step to the initial field, halfway on the propagation path which is five steps from r_0, and the final step of the computation.

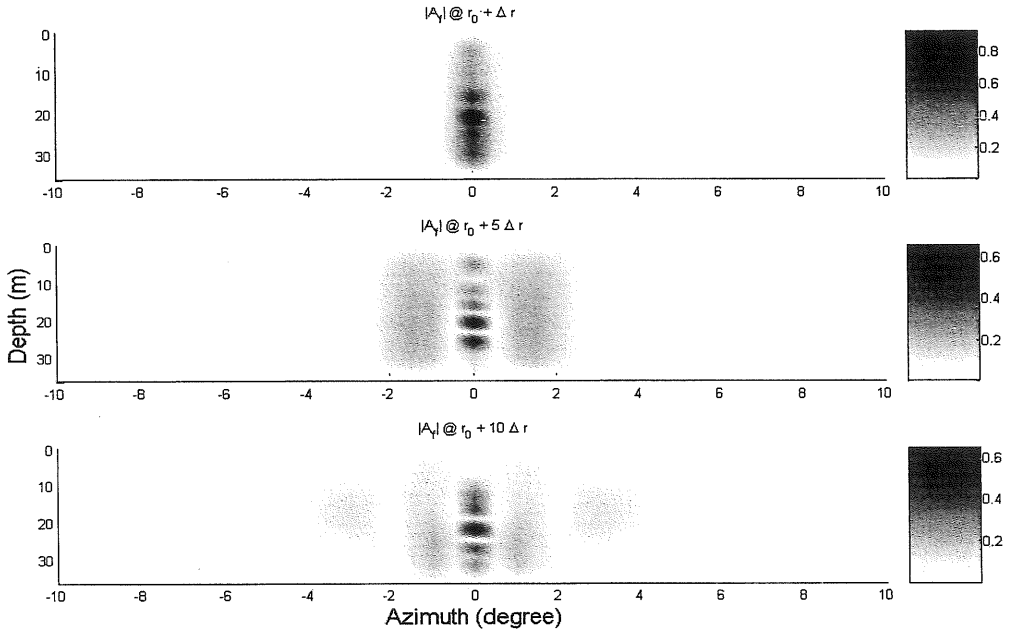

Fig. 4.6 Absolute values of A_f at selected ranges.

From Fig. 4.6 it can be observed that the energy of A_f from the initial field is gradually propagated towards the two side-wall yet a great part of the energy remains at $\theta = 0°$. Note that since the environment is also symmetric with respect to the $\theta = 0°$ plane, the solutions perfectly reveal this symmetry as well.

In Fig. 4.7 the transmitted energy from fluid to solid layer is clear displayed. The energy is continuously input to A_e along the propagation range so that the absolute values are keeping increasing. 3D propagation is also obviously noticed. The results of B_r shown in Fig. 4.7(b) present a major difference from what observed in previous plots of A_f and A_e. The energy does not focus on the central plane but spread out from the plane. Also it is very interesting that at midway on the propagation bath, the energy is less than at the first range step. This has revealed that the energy can not only be transferred into but also output through coupling. Recalling 2D problems where the unknowns can be grouped as two sets, the mathematic or numerical formulations of the wave equations and interface equations have indicated that there is no coupling mechanism between $\{A_f, A_e, B_\theta\}$ and $\{B_r, B_z\}$, and this coupling only exists in 3D problems. Similar outcome can be expected in results of B_z presented in subsequent figure after the plot of B_θ. Similar to the results of A_e plotted in Fig. 4.7(a), the results of B_θ shown in Fig. 4.7(c) reveal the characteristics of energy spreading along the interface but not deep into the bottom. As mentioned in the above discussion of the results of B_r, Fig. 4.7(d) shows expected feature similar to B_r. From

interface equations or numerical formulation, this feature shared by B_r and B_z is due to azimuth coupling at interface and thus is a kind of 3D effect.

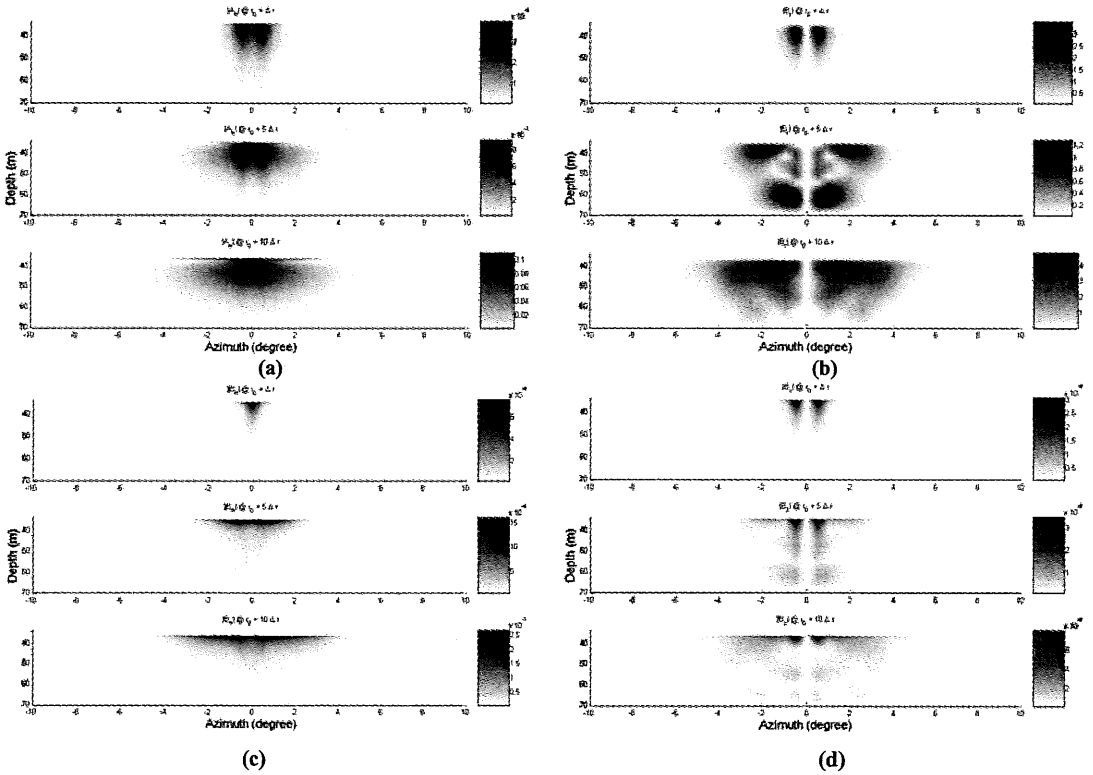

Fig. 4.7 Absolute values of (a) A_e (b) B_r (c) B_θ (d) B_z at selected ranges.

The 3D example tested in this section is highly restrained and simplified to focus on the primary concerns, i.e., realization of the proposed model and how it works with coupled fluid/solid medium with irregular interface. It has to be emphasized that a major difference between considering fluid bottom and real elastic bottom is the demand in computation resources especially the CPU time. This is due to the increasing of the number of physical quantities in elastic bottom, from single one to four. The additional three, B_r, B_θ, B_z, account for shear waves. Under the condition of same grid points, the coefficient matrix considering shear waves is 4×4 times larger than fluid bottom. In other words, the range of interested problem is therefore practically limited. Nevertheless, this kind of technical shortness can be expected to be resolved just like decades ago, and the emphasis must be placed on pursuing the completeness in describing the problem and its solution.

5 Summary

This paper has introduced a modified mathematical model to 3D coupled fluid/solid wave propagation problem and also developed its computational model and a research code. The numerical results produced by this computer code has presented good agreements with analytic solutions which reveals that this computer code produces satisfactory results. The

validation has also shown that the stable marching scheme which implements implicit finite difference method is accurate.

The emphasis has been placed on the development of the numerical model which can solve 3D fluid, elastic, or fluid/solid coupled wave propagation problems. The underlying idea is applying parabolic displacement potential functions to rewrite the wave equations and interface equations, and then using implicit finite difference method to solve the ODE system. Padé series expansion has been used to improve the accuracy in range direction. Since the proposed numerical model and computer code are new, analytical validation of the scheme has been conducted for several problems. The proposed model has been successfully applied to simulate the fluid/solid coupled wave problem.

From both mathematical and numerical modeling, two major differences can be found in 2D/3D comparison, with/without shear effect. A 2D problem is a simplified special case from 3D problems where all the five unknowns $\{A_f, A_e, B_r, B_\theta, B_z\}$ representing the parabolic functions of displacement potentials are coupled together and must be solved simultaneously. The simplest case is 2D problem without shear effect and its unknowns are $\{A_f, A_e\}$ only, that means the energy will be shared by the two quantities only. This is also true for 3D problem without shear effect. If shear effect is to be considered in a 2D problem with only A_f excited by a waterborne source, then the unknowns become $\{A_f, A_e, B_\theta\}$ which means the energy will now be shared by one more quantity, B_θ. Note that if $\{B_r, B_z\}$ is not initially static, then this set of unknowns should also be solved yet as an independent problem so that the solution of $\{A_f, A_e, B_\theta\}$ will not be affected. For the most general case, a 3D problem sustaining shear effect includes all the unknowns $\{A_f, A_e, B_r, B_\theta, B_z\}$, and the energy will shared by these five quantities. In other words, the energy of compressional waves (A_f and A_e) can be overestimated if shear effect is ignored whether in 2D or 3D problems. Also the energy can be overestimated even when shear effect is considered in 2D case, because the energy coupling mechanism between $\{A_f, A_e, B_\theta\}$ and $\{B_r, B_z\}$ is missed. Table 5.1 compares 2D/3D cases with/without shear effect.

Table 5.1 Comparison of 2D/3D cases with/without shear effect.

Shear Effect	2D/3D	Unknown Quantities	Compressional Wave Energy Overestimated
×	2D/3D	$\{A_f, A_e\}$	◎
×	2D	$\{A_f, A_e, B_\theta\}$ and $\{B_r, B_z\}$	○
	3D	$\{A_f, A_e, B_r, B_\theta, B_z\}$	—

3D effects are found to occur from four sources. First, the initial field can decisively affect the propagation pattern including how the waves spread in azimuth direction. Second, the θ-coupling terms (derivatives with respect to azimuth) in the governing equations and interface conditions reflect the constitutional properties of 3D wave propagation. Third, the environment, including the geometry and the acoustic parameters of the medium, has direct influence on the wave propagation path by reflection, refraction, and scattering. Hence a

3D environment will definitely induce 3D effects. Finally, 3D distributed boundaries will induce 3D effects as well.

Although the irregular fluid/solid interface investigated in this dissertation is range-dependent, θ-variation is not considered in the formulation. As Fig. 2.1 shows, the second unit tangent vector $\mathbf{s}(s_r, s_\theta, s_z)$ is set to $(0,1,0)$ so that a cylindrical irregular interface is obtained. In other words, this interface is of axial symmetry and this is why it is drawn as a frustum of right circular cone in Fig. 2.1. This assumption is a serious drawback of the model since such interface will only reflect waves in fixed θ planes, i.e., geometric θ-coupling at interface is ignored. To deal with a real 3D problem, the interface has to be generalized to include variation of bathymetry in θ direction. For example, if the interface as shown in Fig. 2.1 is counterclockwise rotated an angle φ respective to unit direction vector $\mathbf{t}$, then three unit direction vectors are given by

$$\begin{Bmatrix} \boldsymbol{\eta} \\ \mathbf{t} \\ \mathbf{s} \end{Bmatrix} = \begin{bmatrix} -\sin\vartheta\cos\varphi, & -\sin\varphi, & \cos\vartheta\cos\varphi \\ \cos\vartheta, & 0, & \sin\vartheta \\ \sin\vartheta\sin\varphi, & \cos\varphi, & \cos\vartheta\sin\varphi \end{bmatrix}. \tag{4.12}$$

Although a modified mathematical formulation and a novel numerical model for 3D fluid/solid coupled wave propagation problem considering irregular interface this dissertation has been developed and coded as a research prototype program **C4PM**, it is only a beginning for this challenging topic. There are several issues regarding mathematical and numerical enhancements to the modeling and theoretical completeness, namely, wide angle expansion in azimuth, proof of the energy-conserving property such as the proof for LSS wave equation given in Ref. [15]. Each of these issues can be a great improvement and validity proof of the proposed model.

Acknowledgement

This work is supported by National Science Council of Republic of China. The authors would like to thank Dr. Yu-Chiung Teng for her encouragement and discussion.

References

1. Lee, D., Nagem, R. J., Teng, Y.-C., and Li, G. (1996) "A Numerical Solution of Parabolic Elastic Wave Equations," in Proc. 2nd Int'l Conf. Theo. And Comp. Acoust., eds. D. Lee, Y.-H. Pao, M. H. Schultz, and Y.-C. Teng, World Scientific Pub. Co., Singapore.
2. Shang, Er-Chang and Lee, Ding. (1989) "A Numerical Treatment of the Fluid/Elastic Interface Under range-dependent Environments," J. Acoust. Soc. Am., Vol. 85, No. 2, pp. 654 - 660.
3. Lee, D., Nagem, R. J., Resasco, D. C., and Chen, C.-F. (1998) "A Coupled 3D Fluid/solid Wave Propagation Model: Mathematical Formulation and Analysis," Applicable Analysis, Vol. 68, pp. 147 - 178.
4. Sheu, T. W.-H., Chen, S.-C., Chen, C.-F., Chiang, T.-P., and Lee, D. (1999) "A Space Marching Scheme for Underwater Wave Propagation in Fluid/solid Media," J. Comput. Acoust., Vol. 7, No. 3, pp. 185 - 206.

5. Lee, D., Nagem, R. J., and Resasco, D. C. (1997) "Numerical Computation of Elastic Wave equations," J. Comput. Acoust., Vol. 5, No. 2, pp. 157 - 176.
6. Nagem, R. J. and Lee, D. (2002) "Coupled 3D Wave Equations with Fluid/solid Interface: Theoretical Development," J. Comput. Acoust., Vol. 10, No. 4, pp. 431 - 444.
7. Lee, D. and Schultz, M. H. (1995) NUMERICAL OCEAN ACOUSTIC PROPAGATION IN THREE DIMENSIONS, World Scientific, Singapore.
8. Jensen, Finn B., William A. Kuperman, Michael B. Porter, and Henrik Schmidt, (2000) Computational ocean acoustics, Springer-Verlag, New York.
9. Lee, Ding, Pierce, Allan D., and Shang, Er-Chang (2000) Parabolic equation development in the twentieth century, J. Comput. Acoust., Vol. 8, No. 4, pp. 527 - 637.
10. Lee, Ding, and McDaniel, S. T. (1987) Ocean acoustic propagation by finite difference methods, Comp. Maths Applic., Vol. 45, No. 5, special hardcover issue, published by Pergamon, New York (1988).
11. McDaniel, S. T. and Lee, Ding (1982) A finite-difference treatment of interface conditions for the parabolic wave equation: The horizontal interface, J. Acoust. Soc. Am., Vol. 71, No. 4, pp. 855 - 858.
12. Nagem, R. J., Lee, Ding, and Chen, T. (1995) Modeling elastic wave propagation in the ocean bottom, J. Math. Modeling and Scientific Computing, Vol. 2, No. 4, pp. 1-10.
13. Farlow, Stanley J. (1982) Partial Differential Equations for Scientists and Engineers, John Wiley & Sons, Inc., Singapore.
14. Lee, Ding (1974) "Nonlinear multistep methods for solving initial value problems in ordinary differential equations," Ph.D. paper, Polytechnic University of New York.
15. Chen, C.-F., Lee, D., Hsieh, L.-W., and Wang, C.-W. (2005) "A discussion on the energy-conserving property of a three-dimensional wave equation," J. Comput. Acoust., to appear in Vol. 13, No. 4.
16. Hsieh, Li-Wen (2005) "Modeling 3D Wave Propagation in the Ocean Coupled with Elastic Bottom and Irregular Interface," Ph.D. dissertation, National Taiwan University, Taiwan, R.O.C.